Novel orthosteric antagonist of ASIC1a prevents NMDAR-dependent LTP induction.

ARTICLE *in* JOURNAL OF MEDICINAL CHEMISTRY · MAY 2015

Impact Factor: 5.45 · DOI: 10.1021/jm5017329 · Source: PubMed

10 AUTHORS, INCLUDING:

Oleksandr Maximyuk

Bogomolets Institute of Physiology NASU

23 PUBLICATIONS **148** CITATIONS

SEE PROFILE

Volodymyr Sukach

Institute of Organic Chemistry National Acad…

56 PUBLICATIONS **171** CITATIONS

SEE PROFILE

Elena Isaeva

Bogomoletz Institute of Physiology NASU, Ki…

38 PUBLICATIONS **426** CITATIONS

SEE PROFILE

Oleg A Krishtal

Bogomolets Institute of Physiology NASU

172 PUBLICATIONS **5,691** CITATIONS

SEE PROFILE

Journal of Medicinal Chemistry

Article

pubs.acs.org/jmc

Novel Potent Orthosteric Antagonist of ASIC1a Prevents NMDAR-Dependent LTP Induction

Andriy Buta,[†,§] Oleksandr Maximyuk,[†,§,⊥] Dmytro Kovalskyy,[∥,⊥,#] Volodymyr Sukach,[‡,⊥] Mykhailo Vovk,[‡] Oleksandr Ievglevskyi,[†] Elena Isaeva,[†] Dmytro Isaev,[†] Alina Savotchenko,[†] and Oleg Krishtal*[,†,§]

[†]Bogomoletz Institute of Physiology of NAS Ukraine, 4 Bogomoletz Str., 01024 Kyiv, Ukraine

[‡]Institute of Organic Chemistry of NAS Ukraine, 5 Murmanska Str., 02660 Kyiv, Ukraine

[§]State Key Laboratory for Molecular and Cellular Biology, 4 Bogomoletz Str., 01024 Kyiv, Ukraine

[∥]ChemBio Center, Taras Shevchenko University of Kyiv, 67 Chervonotkatska Str., 02094 Kyiv, Ukraine

Supporting Information

ABSTRACT: Acid sensing ion channels 1a (ASIC1a) are of crucial importance in numerous physiological and pathological processes in the brain. Here we demonstrate that novel 2-oxo-2*H*-chromene-3-carboxamidine derivative **5b**, designed with molecular modeling approach, inhibits ASIC1a currents with an apparent IC_{50} of 27 nM when measured at pH 6.7. Acidification to 5.0 decreases the inhibition efficacy by up to 3 orders of magnitude. The **5b** molecule not only shifts pH dependence of ASIC1a activation but also inhibits its maximal evoked response. These findings suggest that compound **5b** binds to pH sensor of ASIC1a acting as orthosteric noncompetitive antagonist. At 100 nM, compound **5b** completely inhibits induction of long-term potentiation (LTP) in CA3-CA1 but not in MF-CA3 synapses. These findings support the knockout data indicating the crucial modulatory role of ASIC1a channels in the NMDAR-dependent LTP and introduce a novel type of ASIC1a antagonists.

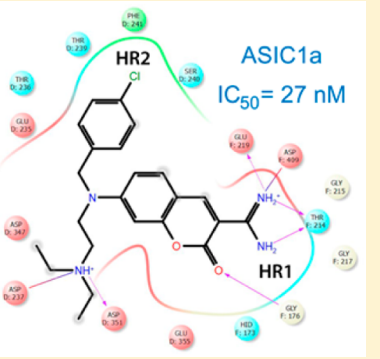

INTRODUCTION

ASIC1a is one of six acid-sensitive ion channels cloned so far from the mammalian nervous system.[1−3] ASIC1a is abundantly expressed in mammalian CNS. It is activated by extracellular acidification and, in contrast to the other ASICs family members, participates in Ca^{2+} signaling: it conducts sodium and calcium ions.[4,5] In most studies, ASIC1a starts its activity at pH 6.9; the amplitude of response grows with the increase of H^+ concentrations up to the saturating pH 6.0.[2,6] It has been shown that in the neurons acutely dissociated from amygdala, ASICs containing ASIC1a subunit are even more sensitive to H^+: they start opening at pH 7.2.[7]

Thus, ASIC1a is an exquisitely sensitive H^+ receptor. This hypersensitivity is crucial for its numerous putative functions in the CNS. It is suggested that higher local concentrations of protons may transiently activate ASICs during normal synaptic activity in the brain.[8,9] There is circumstantial evidence connecting ASICs with certain physiological functions including learning, memory, fear sensing, etc.[1,8,9] Genetic knockout studies show that postsynaptic ASICs are critical for hippocampal CA1−CA3 pathway LTP facilitating NMDA receptor function,[9] but recent data lead to the opposite conclusion.[10] Numerous pathological states including epilepsy, multiple sclerosis, ischemic disorders, traumatic brain injury, depression, spinal cord injury, inflammatory pain, and headache are accompanied by tissue acidosis presumably activating ASIC1a.[1,3,11,12] It has been shown that pharmacological blockage of ASIC1a by amiloride or specific natural blocker PcTx1 as well as its genetic deletion or down regulation affect the above-mentioned pathological states, proving ASIC1a to be a promising molecular target against such disorders. Moreover, precise role of ASICs in numerous physiological processes such as learning, memory, fear sensing, etc. is still underestimated because of the lack of potent and selective small molecule inhibitors. During the past decade several attempts were made to solve this problem (see refs 13−17).

At the moment all of the described ASIC small molecule inhibitors can be divided into three main classes: amiloride and its derivatives, (het)arylamidines, and nonsteroidal anti-inflammatory drugs (NSAIDs).[3,18,19] Well-known potassium-sparing diuretic amiloride which was the first small molecule found to block ASICs[20] is found to be nonselective among different proteins. It blocks the pore of degenerine channel family (ENaC, including ASIC)[21−23] as well as the pore of cyclic GMP-gated cation channel,[24] sodium−hydrogen antiporter 1,[25] T-type calcium channel,[26] and urokinase plasminogen activator,[27] etc. The most potent amiloride derivative inhibits ASIC channels with apparent IC_{50} of 0.49 μM.[16] (Het)arylamidines family comprises first non-amiloride inhibitor A-317567 together with analogs developed by Dubé and colleagues,[13,28] serine protease inhibitor nafamostate used clinically as anticoagulant,[29] fluorescent stain DAPI with other indoleamidines synthesized at Merck,[15] and finally DNA-

Received: November 7, 2014

DOI: 10.1021/jm5017329
J. Med. Chem. XXXX, XXX, XXX−XXX

intercalating bisarylamidines like antiprotozoal drug diminazene or fluorescent dye hydroxystilbamidine.[17,30] Recently, a series of benzothiophenemethylamines and other compounds derived with the help of fragment screening approach were identified as the first non-amidine chemotypes of ASIC inhibitors.[14,31] NSAIDs such as salicylic acid, aspirin, diclofenac, and ibuprofen directly inhibit ASICs in nociceptors but with relatively low potency.[32] Local anesthetics lidocaine and tetracaine are also able to inhibit ASIC currents[33,34] in low millimolar concentrations. Aforementioned small molecule inhibitors were identified through empirical exploratory approach, and their binding sites are yet to be validated. However, for the molecules that resemble structural features of amiloride one might suspect a similar binding mechanism. At the moment, the pharmacology of ASICs still lacks selective and potent inhibitors. New hopes arise with the transition to crystallographic studies of the molecular structure of ASICs. It started with pioneering work carried out by the Gouaux lab.[35]

Crystal structures of chicken ASIC1 (cASIC1) in its different functional states have recently been published revealing structural organization of the homotrimeric channel and conformational rearrangements associated with its function.[35−39] An extracellular domain of ASIC has C_3 symmetry and controls the channel permeability (Figure S1, part A, in Supporting Information). Seven distinct structural domains are arranged in upright forearm and clenched hand manner with only two transmembrane domains, TM1 and TM2, whereas palm, finger, knuckle, β-ball, and thumb domains belong to the extracellular part of the ASIC (Figure S1, parts B and D). The acidic pocket, also referred to as "pH sensor", is formed at the interface of the two ASIC monomers, and because of its C_3 symmetry, three cavities are found per one ion channel (Figure S1, part D). Eleven negatively charged residues Glu98, Glu220, Glu236, Asp238, Glu239, Glu243, Asp260, Asp346, Asp350, Asp408, and Glu354 confer very high electronegative potential to the pocket (Figure S1, part E). They comprise also three carboxylic dyads Glu220/Asp408, Asp238/Asp350, and Glu239/Asp346. Most of these residues are conserved throughout the ASICs family and may be crucial for the ASIC sensitivity to protons.[1,35] The pH sensor has a flasklike shape with the narrow entry expanding inside. From structural domain organization point of view, the thumb, the β-ball, and the finger domains from one ASIC subunit and the palm domain from adjacent subunit contribute residues to form the acidic pocket.[35]

Along with the apo form, complexes of cASIC1 with PcTx1, a highly potent toxin ($IC_{50} \approx 1$ nM),[40] were solved at different pH levels.[37,39] In both cases PcTx1 was found to bind every one of the three pH sensors of the cASIC1. Hydrophobic patch of PcTx1 forms extensive van der Waals contacts with 5-helix of the thumb domain, while its loop II bearing ^{26}RRR^{28} motif extends into the acidic pocket binds to palm, finger, and β-ball domains forming a number of salt bridges and hydrogen bonds.[37,39] Conformational rearrangements of structural domains associated with ASIC function[41] or the toxin binding[37] involve residues from the acidic pocket and its immediate proximity but from various domains. These properties of the pH sensor let us hypothesize that conformational freedom of the pH sensor is a crucial factor in ASIC function and adjusting inherent flexibility of the pocket can modulate the channel activity.

Here we report on design, synthesis, and electrophysiological evaluation of novel 2-oxo-2*H*-chromene-3-carboxamidine blockers aimed to target the pH sensor site of ASIC1a. Most potent novel compounds inhibit hASIC1a currents in nanomolar concentrations with profound dependence of blocking efficacy on the activating pH representing a novel type of ASIC antagonist. We demonstrate that pharmacological inhibition of ASICs by this small molecule prevents LTP induction in hippocampal CA3−CA1 pathway, thus supporting the important physiological role of ASICs in the plasticity of the mammalian brain.

RESULTS

Chemistry. Compounds **1**−**5** were synthesized (Scheme 1) starting from *N*,*N*′-dialkyl-3-aminophenoles **7a**−**f** obtained in

Scheme 1. General Scheme for the Synthesis of Compounds 1−5[a]

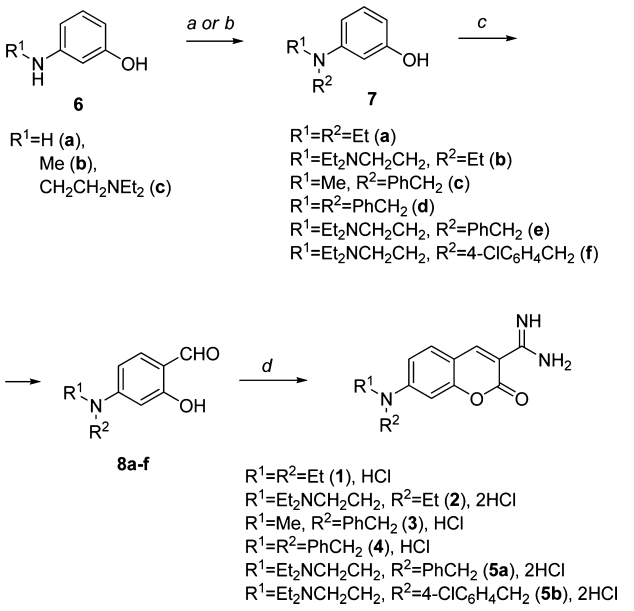

[a]Reagents and conditions: (a) $PhCH_2Br$, $NaHCO_3$, MeCN, 40 °C, 4 h; (b) EtI, $PhCH_2Cl$ or 4-$ClC_6H_4CH_2Cl$, MeCN, 81 °C, 3 h; (c) $POCl_3$, DMF, 80 °C, 6 h; (d) $NCCH_2CO_2Et$, $AcONH_4$, EtOH, 78 °C, 15 min.

turn by alkylation of known 3-aminophenoles **6a**−**c**.[42] Subsequent Vilsmeier−Haack formylation furnished corresponding aldehydes **8a**−**f** which were converted into target 2-oxo-2*H*-chromene-3-carboximidamides **1**−**5** (as mono- or dihydrochloride salts) by cyclocondensation with ethyl cyanoacetate using the procedure developed by Sakurai et al.[43]

Electrophysiological Evaluation. The potency of compounds was evaluated on hASIC1a channels endogenously expressed in HEK 293 cells using standard patch-clamp technique.[44] In response to a pH drop from 7.4 to 5.0, approximately 80% of the cells were clamped at −100 mV gated ionic current ranging from 200 pA to 1 nA which is mediated by homomeric hASIC1a channels.[45]

Development of pH Sensor Binding Antagonists of ASIC1a. The crystal structure of the cASIC1[35] allowed us to perform a rational structure based design of small molecule antagonists. Homology modeling was used to construct the spatial model of human ASIC1a (hASIC1a). High overall sequence identity (>90%) and particularly in the pH sensor (only two amino acids differ) between human and chicken

DOI: 10.1021/jm5017329
J. Med. Chem. XXXX, XXX, XXX−XXX

ASIC1 allowed us to obtain a model of the hASIC1a with a virtual X-ray level of confidence.

We have performed unbiased docking of a small molecule diversity set of 10 000 compounds into the pH sensor saving 5 poses per ligand, as initial attempt. Whole pH sensor cavity was treated as the binding site. Processing of the generated poses did not reveal any clear preference either toward binding mode or toward a particular chemical scaffold. In the vast majority of generated poses small molecules bound alongside the acidic pocket wall, which is similar to the binding to a flat protein surface. Electrophysiological evaluation of the top 10 molecules did not reveal the molecules active at concentration as high as 100 μM.

At the next step, we tried to mimic PcTx1 in the acidic pocket with small molecules that would resemble its key contacts. The guanidine group of PcTx1 Arg27 in the channel–toxin comlex[37,39] is found to be in tight environment of carboxyl groups of cASIC1 Glu220/Asp408 dyad and oxygens of cASIC1 Thr215, Gly216, and Gly218. Side chains of Arg27 of toxin form van der Waals contacts with Phe174. Arg28 of PcTx1 binds Glu243 and Phe242 side chains of ASIC1, forming salt bridge and cation–π interactions, respectively. Finally, residue Arg26 forms a hydrogen bond with Asp350.[37,39] The ^{26}RRR^{28} motif efficiently spans through palm, finger, and thumb domains pointing to the tri-star topology of putative antagonist, which would be able to fill the acidic pocket and reach its distal domains (Figure 1). To test this hypothesis, we conducted

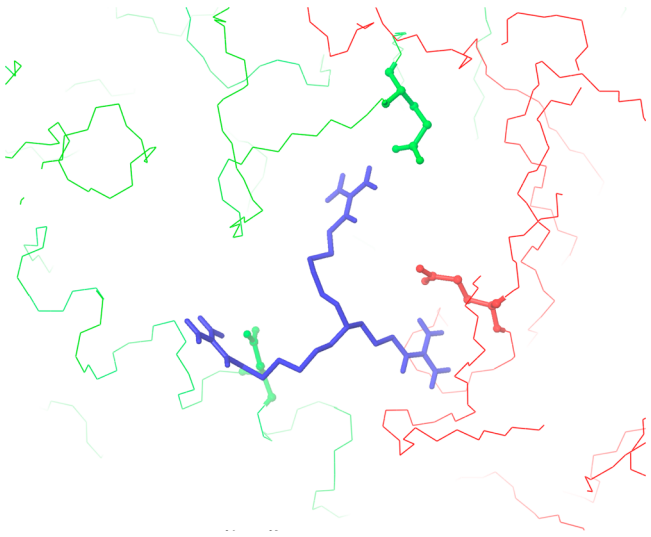

Figure 1. Interaction of the ^{26}RRR^{28} motif of PcTx1 with pH sensor of ASIC1a. The motif interconnects three domains and two subunits, which impairs motions with respect to each other. PcTx1 atoms are shown in blue; two ASIC subunits are shown in red and green. For clarity only N and C atoms of the backbone are shown. Arg26 binds to the Asp350 from the thumb domain. Arg27 binds underneath Glu220 of the palm domain from adjacent subunit. Arg28 reaches Glu243 from finger domain.

iterative structure guided design of a new blocker that would efficiently bind amino acids from palm, finger, and thumb domains within the acidic pocket.

We used recently published 2-oxo-2*H*-chromene-3-carboxamidine scaffold[46] as template for the design of novel putative ASIC antagonists possessing the above-mentioned tri-star topology. First 2-oxo-2*H*-chromene-3-carboxamidine derivative, compound **1**, inhibited hASIC1a current to 41.0 ± 3.6% (n = 4) at 100 μM (Table 1). Binding modes of compound **1** evaluated with docking showed little preference to a particular position within the acidic pocket; however, we identified frequently visited sites that might denote preferable interactions. Most favorably, the amidine group binds to the two cavities. One of them is formed by residues from the palm domain only (Thr214-Glu219, His173-Gly176, and Glu355), whereas the residues Glu97, Asp259, Try191, and Asp237-Ser240 contribute to the other one.

Next, we introduced flexible tertiary amino group (compound **2**) to improve anchoring of the putative antagonist to the charged groups in the acidic pocket. Surprisingly, compound **2** had even weaker blocking activity than compound **1** possibly because of the large desolvatation penalty that unfavorably contributes to the free energy of binding. In contrast, introduction of the benzyl group at the 7-amino position (compound **3**) had positive impact on antagonizing potency (36.6 ± 5.6%, n = 4, similar to that observed with compound **1**) (Table 1). To define the possible site of benzyl group binding, we estimated hydrophobic sites in the acidic pocket using SiteMap.[47] There are only two regions in the pH sensor that exhibit hydrophobic propensity. The hydrophobic region 1 (HR1) is located between residues Thr214 and Gly176 of the palm domain and is formed by backbone atoms of corresponding residues. Another region with hydrophobic propensity (HR2) was attributed to the cavity formed by noncharged atoms of residues Glu235-Phe241. Docking of compound **3** revealed that its benzyl group binds to the HR2 and forms van der Waals contacts with Cβ of the Glu235 and Cζ of Phe241. However, the inhibition efficacy of compound **3** was found to be virtually the same as for compound **1** (see Table 1). In order to bind both apolar cavities, we synthesized compound **4** with two benzyl groups at the 7-position of the coumarin core. Unfortunately, this compound was insoluble suggesting that the second substituent at nitrogen atom position 7 should preferably contribute to efficient polar interactions. Docking of compound **5a** bearing both tertiary amine fragment and benzyl substituent to the acidic pocket revealed a preference toward a binding pose where the coumarin moiety binds to HR1 cavity with amidine group forming extensive hydrogen bonds with Thr214, Glu219, and Asp408, similar to what was observed with compound **1**. Carbonyl oxygen forms an additional hydrogen bond with NH of Gly176 and van der Waals contacts with imidazole of His173. Positively charged tertiary nitrogen of compound **5a** binds carboxylates of the Asp237/Asp351 dyad, and benzyl group points toward the second hydrophobic site (Glu235-Phe241), similar to compound **3**. In this mode, both hydrophobic patches of the acidic pocket were addressed as well as the carboxyl dyad Asp237/Asp351. This, along with the better filling of the pocket, could lead to the improved interaction with ASIC1a.

The derivative **5a** caused substantial inhibition of hASIC1a current down to 28.2 ± 4.2% and 65.7 ± 4.7% at 100 and 10 μM, correspondingly (Table 1). Lowering the concentration of **5a** to 100 nM resulted only in negligible inhibition (96.1 ± 3.2%, n = 12) of hASIC1a currents (Table 1). Its activity is comparable with other reported small molecule ASIC1a blockers (such as amiloride, nafamostat, A-317567, etc.). It should be noted that all the observed blocking effects were fully reversible.

Careful evaluation of the above binding mode revealed that the benzyl moiety of compound **5a** does not fill the

DOI: 10.1021/jm5017329
J. Med. Chem. XXXX, XXX, XXX–XXX

Table 1. Inhibition of ASIC1a Currents by 2-Oxo-2*H*-chromene-3-carboxamidine Derivatives at Different Concentrations and Activating pH Values

compd	R1	R2	concn	inhibition at pH 5.0 (%)	inhibition at pH 6.7 (%)
1	Et	Et	100 μM	41.0 ± 3.6	49 ± 4.2
2	$Et_2NCH_2CH_2$	Et	100 μM	78.7 ± 3.6	53.2 ± 3.3
			10 μM	101.3 ± 3.9	77.5 ± 4.4
3	Me	$PhCH_2$	100 μM	36.6 ± 5.6	22.3 ± 3.3
			10 μM	79.2 ± 9.3	42.9 ± 2.6
4	$PhCH_2$	$PhCH_2$	10 μM	NS[a]	NS[a]
5a	$Et_2NCH_2CH_2$	$PhCH_2$	100 μM	28.8 ± 4.2	3.7 ± 4.5
			10 μM	65.7 ± 4.7	22.1 ± 3.3
			100 nM	96.1 ± 3.2	68.9 ± 4.8
5b	$Et_2NCH_2CH_2$	4-$ClC_6H_4CH_2$	10 μM	44.8 ± 4	2.5 ± 5.4
			100 nM	98.6 ± 2.4	23.7 ± 4

[a]NS: not soluble. All the compounds were obtained as (di)hydrochloride salts.

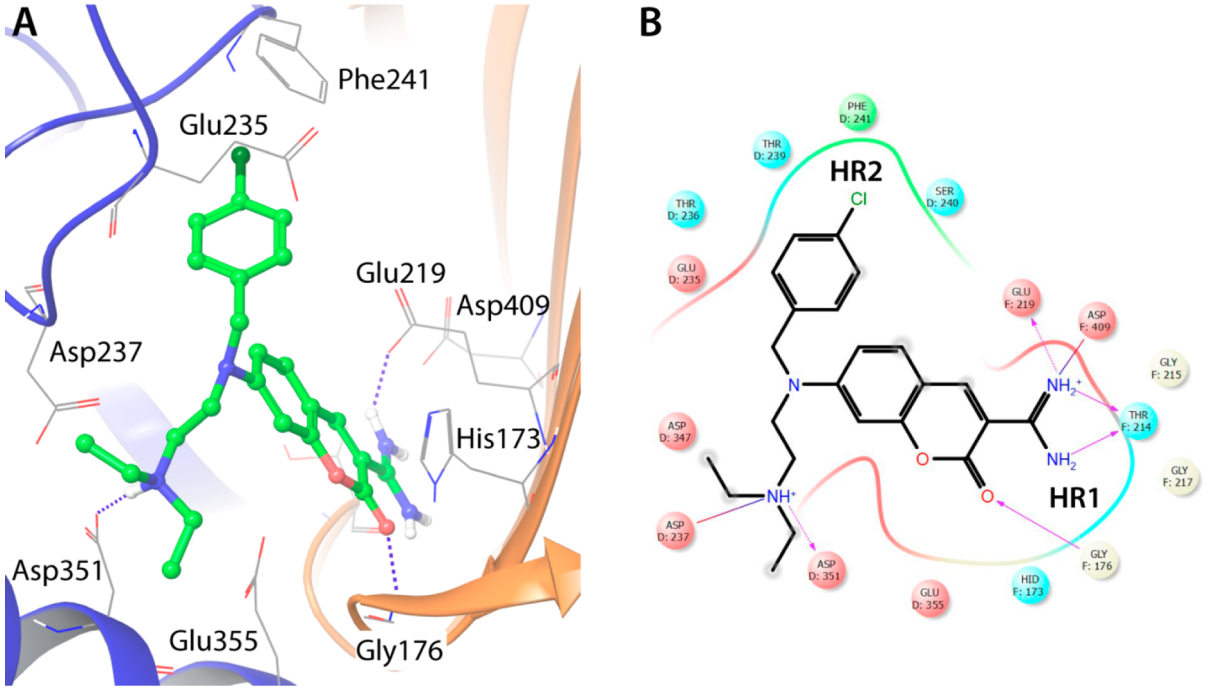

Figure 2. Interaction model of compound **5b** with human ASIC1a. (A) Compound **5b** binds to the pH sensor. Most important residues for the interaction with the blocker are shown as wires. Ribbons are colored after chain name. Coumarin core binds to the palm domain of one subunit. *p*-Chlorobenzyl and diethylamino moieties bind to the finger and thumb domains at the adjacent subunit, respectively. (B) Schematic contact map of compound **5b** and the acidic pocket. Residues that contribute to the polar, apolar, and cation−π interactions are shown. Regions with hydrophobic propensities are denoted as HR1 ans HR2 (see Results).

hydrophobic cavity efficiently and the extra space is available. Shortest distance between backbone heavy atoms of the Phe241 and carbon in para position of the benzyl group of **5a** is 5.31 Å, indicating that a halogen atom may fit this space. Introduction of the chlorine atom in the para position of the benzyl group (compound **5b**, Figure 2) further improved the blocking potency of the molecule (44.8 ± 4.0%, n = 9 at 10 μM for **5b** vs 65.7 ± 4.7%, n = 10 for **5a**). The observed increase in the efficacy supports the suggested binding mode of compound **5b**.

We also have tested the potency of compound **5b** to inhibit native ASIC currents on hippocampal neurons of rat and found that 10 μM compound inhibited rASIC1a-like down to 48.3 ± 5.0% (n = 4). The experiments on DRG neurons of rat revealed that compound **5b** induces virtually the same inhibition of fast rASIC3-like currents (45.2 ± 4.3%, n = 4) but not of the slow rASIC2-like currents (99.3 ± 1.3%, n = 3).

Potency of the 2-Oxo-2*H*-chromene-3-carboxamidine Derivatives Depends on the Acting pH Level. All the 2-oxo-2*H*-chromene-3-carboxamidine derivatives have been designed to target the pH sensor of ASIC1a, the most sensitive to protons place in the receptor.[1,35] One should expect that the binding efficacy of the described compounds depends on pH. In order to check this hypothesis, all compounds derived in this study were evaluated at pH 6.7 and pH 5. As expected, a profound difference was observed between these sets of data. The ionic current elicited by a shift to pH 6.7 had much slower activation, smaller amplitude, and slower desensitization onset as compared to the current at pH 5.0. This current was notably inhibited by 100 nM compound **5a** (68.9 ± 4.8, n = 10, Table 1) as compared to insignificant (96.1 ± 3.2%; n = 12)

DOI: 10.1021/jm5017329
J. Med. Chem. XXXX, XXX, XXX−XXX

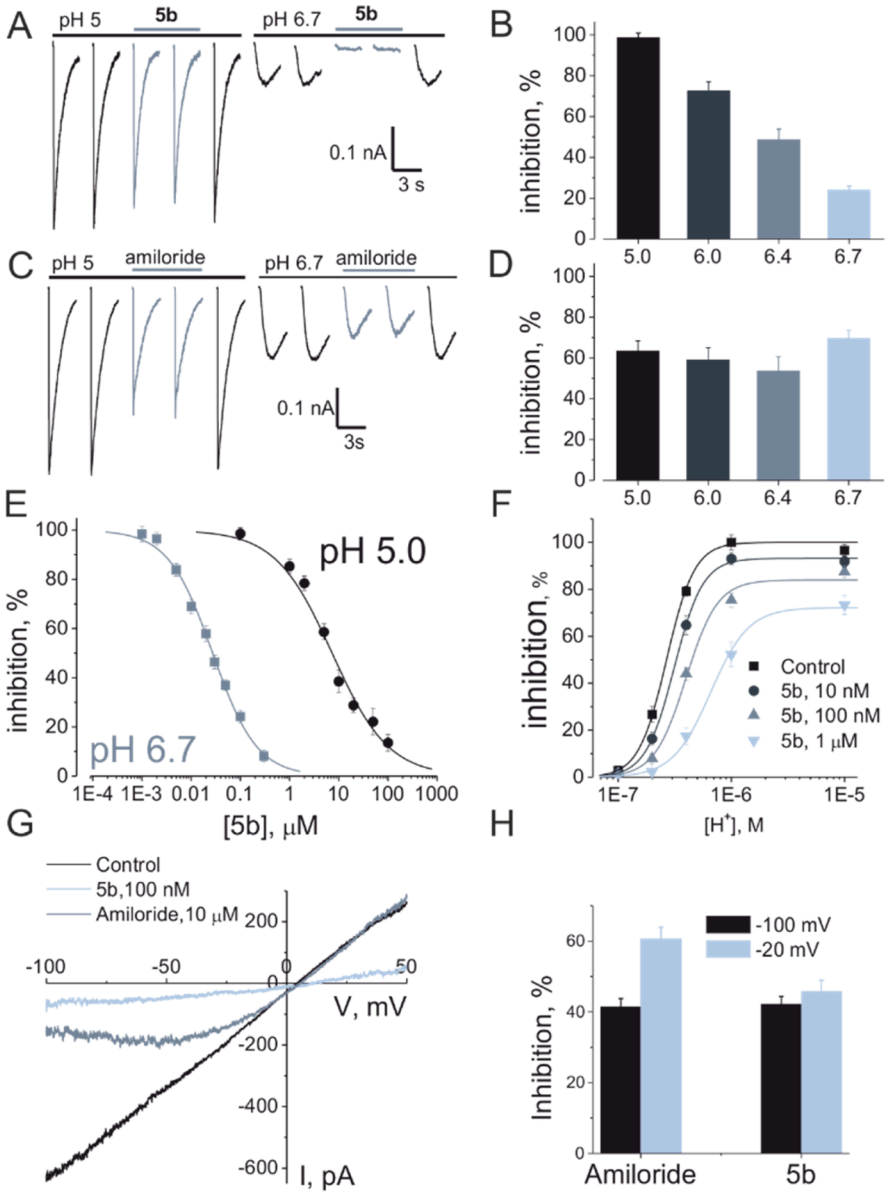

Figure 3. Compound **5b** inhibits ASIC1a currents depending on acting pH in nanomolar concentrations when the channels are activated by mild pH changes. (A) Representative current traces of ASIC1a currents in HEK 293 cells activated by varying pH drops from basal pH 7.4 in control conditions and under exposure to 100 nM compound **5b**. (B) Summary data for the inhibition of ASIC1a currents by compound **5b** at different activating pH are shown. (C, D) Similar experiments as shown in (A) and (B) were made for inhibition ASIC1a currents by channel blocker amiloride for comparison. (E) Dose−response relationships measured for the inhibition of ASIC1a currents by compound **5b**. The ASIC1a current was elicited by pH drop from 7.4 to 6.7 (gray squares) and from pH 7.4 to 5.0 (black circles). (F) Steady-state activation curves for ASIC1a currents measured in the control and in the presence of indicated concentrations of compound **5b**. ASIC1a current amplitudes were normalized to the maximal evoked response measured without compound **5b** in the bathing media. (G) *I*−*V* relationships in control, in the presence of 100 nM compound **5b**, and in the presence of 10 μM amiloride measured by slow ramp protocol (velocity 0.1 mV/ms) at the peak of ASIC1a current elicited by a drop of pH to 6.7. (H) Inhibition of ASIC1a currents caused by 100 nM compound **5b** vs 10 μM amiloride at indicated voltages.

inhibition observed at pH 5.0. Compound **5b** was found to be even more potent at pH 6.7 (100 nM, 23.7 ± 4.0% n = 14), whereas at pH 5.0 this concentration was virtually inactive (98.6% ± 2.4, n = 7). Pronounced pH-dependence of its inhibition compared with classical ASIC pore blocker amiloride is demonstrated in Figure 3 (AB for **5b** and CD for amiloride). Correspondingly, a profound leftward shift of the dose−response relationship for compound **5b** was observed when ASIC1a currents were activated by pH 6.7 as compared to pH 5.0 (Figure 3E, IC_{50} =27.35 ± 1.23 nM, n = 7−9 vs 7.34 ± 0.84 μM, n = 8−10 at pH 6.7 and pH 5.0, correspondingly). As well as in all previous cases, inhibition by compound **5b** was fully reversed within a few minutes of washout.

ASIC1a Is Antagonized by 5b through an Orthosteric Noncompetitive Mechanism. A few decades ago, it was shown that amiloride produces the voltage-dependent non-competitive blockage of ASIC currents entering, in all probability, the pore of the channel.[20] We have evaluated the potency of compound **5b** vs amiloride at different membrane voltages. Amiloride blocked ASIC1a current to 41.34 ± 2.42% (n = 7) at −100 mV, while changing holding voltage to −20 mV decreased this blockade to 60.70 ± 3.23% (n = 6, p =

DOI: 10.1021/jm5017329
J. Med. Chem. XXXX, XXX, XXX−XXX

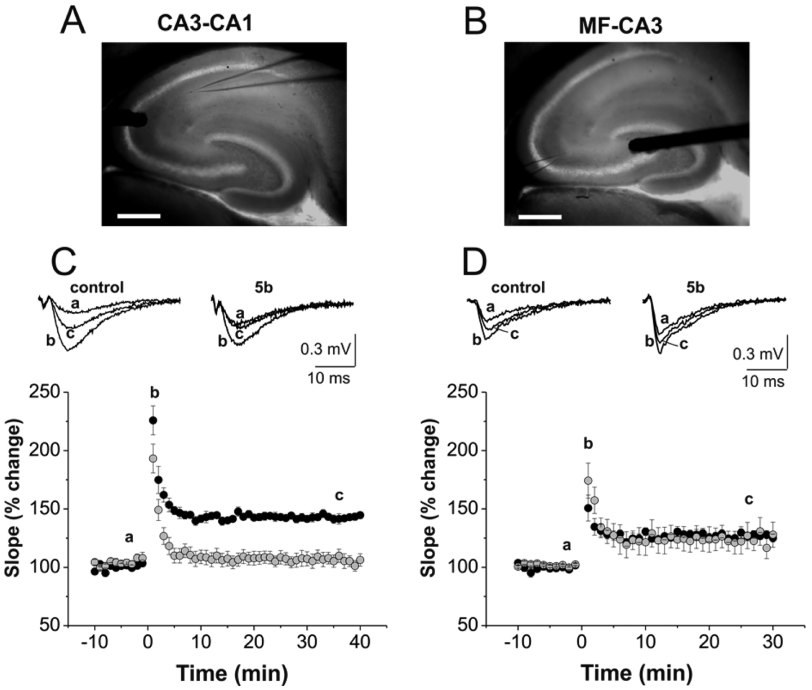

Figure 4. Effect of bath application of compound **5b** on long-term potentiation. LTP was recorded in two synaptic pathways of hippocampal circuitry: CA3-CA1 (A) and MF-CA3 (B). fEPSPs were evoked by stimulation of Shaffer collaterals (A) or mossy fibers (B) using concentric electrode. They were recorded using a glass electrode filled with extracellular solution placed in CA1 stratum radiatum (A) or CA3 stratum lucidum (B). Scale bar, 0.5 mm. (C, D) Average of baseline-normalized initial slopes of fEPSP evoked by stimulation of Shaffer collaterals (C) or mossy fibers (D) before and after delivery of high-frequency stimulation in control (black) and in the presence of 100 nM of compound **5b** (gray) in the external medium. Upper panels: sample records of fEPSP measured at baseline (a), at 2 min (b), and at 30 min (c) post-tetanus. All data are presented as the mean ± SEM.

0.0006). However, compound **5b** produced similar inhibition at both these voltages, 42.12 ± 2.26 (n = 8) and 45.78 ± 3.13 correspondingly (n = 9), indicating the absence of voltage dependence of blocking action (Figure 3H, p = 0.92). Current/voltage relationships for amiloride and compound **5b** show that blocking potency of amiloride is decreased with depolarization of cellular membrane, whereas the potency of compound **5b** remains unaltered (Figure 3G). These data suggest that the location of the binding site for **5b** is at extracellular domains of the channel but not within the cellular membrane.

Compound **5b** affects steady-state activation of ASIC1a current (Figure 3F). At the concentration of 10 nM, it shifted the dose−response curve to a lower pH range (EC_{50} = 6.57 ± 0.01 pH, n = 7−8 in control and EC_{50} = 6.50 ± 0.01 pH, n = 8−10 in the presence of 10 nM compound **5b**). It is worth noting that at saturating pH a small inhibition of maximal evoked response was observed already at this small concentration of **5b** (93.18 ± 1.04% of control). At higher concentrations of this compound the rightward shift of the dose−response curve became more significant (EC_{50} = 6.40 ± 0.03 pH, n = 6−9 at 100 nM and EC_{50} = 6.18 ± 0.05 pH, n = 5−8 at 1 μM) and the maximal evoked response was markedly reduced to 83.94 ± 4.25% at 100 nM and 72.19 ± 5.21% at 1 μM. The dose−response shift accompanied by maximal evoked response inhibition is characteristic for orthosteric non-competitive or negative allosteric modulation mechanism.[48]

Compound 5b Affects Long-Term Synaptic Plasticity in Hippocampus. Previous reports indicate that ASICs can play a substantial role in synaptic plasticity, learning, and memory.[9] We have examined the effect of rASIC1a blockade on CA3−CA1 pathway. First, we evaluated the potency of compound **5b** to inhibit rASIC1a channels in isolated pyramidal hippocampal neurons of rats. At 100 nM, compound **5b** induced substantial inhibition of rASIC1a-like currents down to 9.39 ± 2.9% (n = 4, p < 0.0001), whereas at 1 μM it did not block the main ionic currents involved in synaptic transmission (Figure S2). Application of compound **5b** (100 nM) did not affect the slope and amplitude of field excitatory postsynaptic potential (fEPSP) at CA3−CA1 synapses (103.4 ± 3.4%, p = 0.4 for the slope and 104.6 ± 3.0%, p = 0.2 for the amplitude correspondingly, n = 8). Moreover, 10-fold higher concentration of compound **5b** did not result in the appearance of any feasible inhibition of amplitude for both inhibitory and excitatory postsynaptic currents (Figure S3). Immediately following high-frequency stimulation **5b**-treated as well as control slices showed the increase in fEPSP slope and amplitude (short-term potentiation, STP). The degree of STP in **5b**-treated and control slices was not significantly different (193.2 ± 12.3%, n = 9 vs 225.9 ± 12.4%, n = 8, correspondingly, p = 0.08). As shown in Figure 4C, application of compound **5b** occluded LTP in CA3−CA1 synapses (142.9 ± 2.5%, n = 9 in control vs 106.2 ± 5.2%, n = 9 in **5b**-treated slices, p < 0.0001). These data are in agreement with previous studies suggesting that activation of postsynaptic ASICs promotes the membrane depolarization and thereby facilitates NMDA receptor function and contributes to LTP.[9,49] With this hypothesis in mind, we examined the effect of compound **5b** on NMDAR-independent LTP. The synapses formed by the mossy fibers (MF) on CA3 neurons exhibit a form of experience-dependent synaptic plasticity that is induced and expressed presynaptically and does not depend on the activation of NMDA receptors.[50] To study the effect of

DOI: 10.1021/jm5017329
J. Med. Chem. XXXX, XXX, XXX−XXX

compound **5b** on LTP in MF-CA3 pathway we used a modified protocol for LTP induction (4 bursts of 100 stimuli delivered at 100 Hz with a 2 min intervals). All experiments were performed in the presence of NMDA receptor blocker MK-801. Figure 4D represents group data for fEPSPs evoked by stimulation of MF and recorded in CA3 region of hippocampus in control and in **5b**-treated slices before and after delivery of tetanic stimulation. Repeated-measures ANOVA revealed that there was no significant difference in the LTP level between control and **5b**-treated slices ($118.3 \pm 9.6\%$ [$n = 10$] vs $117.0 \pm 11.4\%$ [$n = 12$], $p = 0.98$), supporting the idea that ASIC1a specifically contributes to the NMDAR-dependent plasticity.

DISCUSSION

The ion channel activated by extracellular H^+ was found first in mammalian sensory neurons and initially was associated with nociception.[51−53] However, after cloning the family of ASICs[2,54−57] it became apparent that these channels play very diverse roles in much broader repertoire of physiological mechanisms and pathological conditions.[1,12,58−61] Homotrimeric ASIC1a channel[2] is a specific brain sensor for protons considered to be the key participant in learning, memory, and fear sensing as well as an important player in different pathological states, such as epilepsy, multiple sclerosis, ischemic stroke, traumatic brain injury, depression, spinal cord injury, inflammation, and headache.[1,3,7−9,11,12,58] Hence, the involvement of ASICs in such a wide range of disorders urges a development of ASIC blockers as therapeutic agents.

Compound screening remains the main source of new blockers of ASICs. However, low throughput of such screening largely limits the progress. The main efforts of medicinal chemistry are focused around amiloride and (het)arylamidine derivatives.[13−17,28,31,46] As a result, current small molecule ASIC inhibitors are largely a combination of amidine or guanidine groups with aromatic moieties, while the bioisosteric replacement strategy may result in new heterocyclic scaffolds.[31,46] Largest caveat of the discovered compounds is their promiscuity among targets other than ion channel. This imposes substantial hurdle on the further development.[14]

To our knowledge, there are still no studies utilizing the structural information on the ASIC despite recent advances in solving X-ray of ASIC1a.[35−39] The present study has been commenced upon disclosure of the first structure of ASIC, chicken ASIC1 in the desensitized form.[35] We decided to focus our efforts on the acidic pocket located in the extracellular domain of ASIC1a. Its three features favored our choice. First, the crystal structure of ASIC1 revealed that 4 out of 5 structural domains located above cellular membrane contribute to the acidic pocket, suggesting that its flexibility may be important for the channel function. Second, the pocket is heavily saturated with negatively charged residues; some of them are invariant and crucial for pH sensitivity. Third, highly potent toxin, PcTx1[40] binds the pH sensor.[37,38] From these facts we hypothesized that altering conformational perturbations of the pocket may impair function of the whole ion channel. In silico assessment of the small molecule compound library against the acidic pocket resulted in very diverse binding orientations of the compounds that reflect large discrepancy in sizes of ligands and the pocket. Patch clamp validation of top scored 10 compounds returned no active molecules. Design of specific compounds directed to fill volumetric pH sensor would be preferable strategy then. To address size, we analyzed binding mode of PcTx1 to the ASIC1a, especially its pH sensor buried part, ^{26}RRR^{28} motif.[37,39] We choose the tri-star shape as the key feature required by a small molecule to take advantage of the roomy acidic pocket.

The antagonist design was based on 7-amino-2-oxo-2*H*-chromene-3-carboxamidine core, since its amino group could be functionalized with two substituents providing an origin for divergent nonlinear structures. Compound **1** showed a weak blocking activity, yet comparable to the nafamostate metabolite,[29] NSAIDs,[32] and local anesthetics.[33,34] Similar to amiloride, compound **1** was too small to possess a single preferred position in the acidic pocket and modeling of the feasible poses resulted in diverse variants guided by binding of amidine group to carboxylates. Introduction of the flexible polar (compound **2**) and aromatic (compound **3**) groups was aimed at anchoring the small molecule with specific interactions. Electrophysiological screening of derivatives **2** and **3** at pH 5.0 showed a clear preference of hydrophobic substituent over polar. The acidic pocket of ASIC1a is depleted in lipophilic residues so that the in silico assessment of plausible binding of compound **3** reveals reduced number of poses compared to compound **2**. Primary binding site for benzyl moiety was identified as hydrophobic cavity centered at phenyl ring of Phe241 from the finger domain.

All the compounds **1**−**3** did not have two bulky substituents at position 7 that would result in the efficient filling of the acidic pocket volume. Our attempt to introduce a second benzyl group to coumarin unfortunately led to the insoluble compound **4**. In order to balance compound potency with its solubility, we combined compounds **2** and **3** resulting in compound **5a**. Substantial potency increase suggested that bulky groups are beneficial for the putative ASIC1a antagonist. The difference is even more striking, since compound **2** is largely depleted in activity. This fact can be rationalized by the predicted binding mode. Compound **5a** binds both hydrophobic regions HR1 and HR2 with its aromatic moieties, deep in the acidic pocket (Figure 2). The remaining amino arm is pointed outward to interact with Asp237/Asp351 dyad or Glu355. In general, charged interactions are beneficial for the free energy of binding, when they are prepositioned to each other.[62] Final compound **5b** was designed to enhance interaction with residue Phe241, and its improved activity supports the suggested binding mode: the compound is presumed to interconnect palm, finger, and thumb domains of the ASIC through coumarin core and benzyl and amino moieties, respectively.

Conformational rearrangements of ASIC structural domains are crucial for all transitions between open, closed, and desensitized states. Mutation of charged residues located in proximity to the acidic pocket and involved in interdomain contacts led to the substantial change in pH sensitivity.[63] Hill coefficient in mutants Asp350Asn[37] (chicken analog of Asp351) and Glu355Gln[63] was substantially lower than in wild type ASICs. Both these residues are located at the pocket entry and are targeted by tertiary amine moiety of compound **5b**. Phenylalanine at position 241 is absolutely invariant among all ASIC species, highlighting the functional importance of the structural motif. Residues Glu235 and Glu355 are largely involved in the close → open transition,[41] and binding to these residues might substantially interfere with this transformation. Interaction of the amidine group with the first hydrophobic cavity is facilitated by the network of hydrogen bonds and van der Waals contacts. Four hydrogen bonds formed by amidine group and lactam oxygen with Thr214, Glu219, and Gly176 are

DOI: 10.1021/jm5017329
J. Med. Chem. XXXX, XXX, XXX−XXX

enhanced with van der Waals contacts and $\pi-\pi$ interaction of coumarin core with imidazole ring of His173. Position of His173 is variable between ASIC subtypes and can be used to gain specificity between them. For instance, in human ASIC3 arginine is found in equivalent position and its flexibility may interfere with such binding mode of compound **5b**.

Recently published structure of the complex of chicken ASIC1a with PcTx1 revealed that hydrophobic regions HR1 and HR2 and carboxyl dyad on the α-helix from the thumb domain are both addressed by the toxin.[37,39] Orientation of the coumarin core is very similar to the conformation of the side chain of Arg27 (Figure S4). Side chain of Arg27 extends into the acidic pocket along palm domain residues with guanidine group binding to the HR1 in the position nearly identical to the amidine group of compound **5b**. Carbon atoms of the Arg27 side chain also form van der Waals contacts with Phe174 (numbering of chicken ASIC1). In both crystals, Arg28 binds Glu243 and Phe242 side chains, forming salt bridge and cation$-\pi$ interactions In the case of **5b** *p*-chlorobenzyl enhanced van der Waals contacts with Phe241. Finally, residue Apr26 forms hydrogen bond with Asp350[37,39] similar to the tertiary nitrogen of compound **5b**. PcTx1 forms tight interactions with residues from thumb, palm, and finger domains, altering flexibility of the channel molecule. Such overlap in the predicted binding mode for compound **5b** and crystal structure of the channel−toxin complex is not surprising, since 2-oxo-2*H*-chromene-3-carboxamidine derivatives developed in this study were designed to occupy the same place with PcTx1 in pH sensor of ASIC1a channel and therefore antagonize its activity via orthosteric mechanism. As it was shown long before the exploration of PcTx1 binding mode,[37,38] this toxin, when bound to the channel, slightly shifted the activation and desensitization curves to lower H^+ concentrations[64] because of the increase in the apparent affinity to H^+. Later it was shown that the interaction of PcTx1 with ASIC1 channel is state-dependent: PcTx1 binds more tightly to the open state of the ASIC1b channel than to the closed and desensitized ones and facilitates openings of the channel. In the case of ASIC1a, it binds most tightly to the open and the desensitized state, promoting desensitization.[65] Therefore, a molecule bound to the pH sensor may well modify ASIC1a channel sensitivity to H^+ as well as its gating mechanism. Here we show that the compound affinity increases with the change in activating pH from 5.0 to 6.7 (Figure 3E). Thus, it looks like the compound competes with H^+ for the binding site like Ca^{2+} ions.[6] At any concentration, compound **5b** promotes both rightward shift of dose−response curve and reduction of maximal evoked response, showing a behavior typical for negative allosteric modulator or orthosteric noncompetitive antagonist (Figure 3F, dose−response curves performed in the absence or presence of **5b**). 2-Oxo-2*H*-chromene-3-carboxamidine derivatives were designed to target the pH sensor of ASIC1a. We demonstrate that the affinity to H^+ is modulated by compound **5b** (Figure 3E) as well as the affinity of compound **5b** depends on activating pH (Figure 3F), suggesting that the molecule competes with H^+ for the pH sensor. These data serve in fact as a proof of a concept: novel compounds interact with pH sensor. However, the observed relationships do not fit a competitive inhibition mechanism. The latter requires that antagonist bound to receptors must dissociate quickly enough to be substituted by the agonist presented at the receptor compartment.[48] In the other case the antagonist will occupy an inordinately high percentage of the receptors and antagonism will dominate. If the percentage of occupied receptors is high enough, the agonist does not produce a maximal response.[48] This is just the case of compound **5b** inhibition. We speculate that *p*-chlorobenzyl group of **5b** providing rich van der Waals contacts with Phe241 in the acidic pocket of ASIC1a greatly decelerates dissociation of **5b** from receptor resulting in observed orthosteric noncompetitive inhibition.

Thus, compound **5b** is most effective at slight acidifications. Various pathological states, such as ischemic stroke, epilepsy, inflammation, etc., are characterized just by mild acidification of the tissue. Such minor drop in extracellular pH from 7.4 to 6.8 is sufficient for significant membrane depolarization accompanied by the trains of action potentials.[66] The activity of ASIC1a channels induced by different pathological states leads to neuronal death.[1,3,11,12] Recently it has been suggested that H^+ acts as neurotransmitter in amygdala;[49] the novel ASIC antagonists will help to further elucidate the role of ASICs in neurotransmission.

In conclusion, we have identified a plausible structural motif for the small molecules acting as orthosteric noncompetitive antagonists of ASICs. Mutagenesis and deeper SAR studies will be needed to further improve the ASIC blockers, but even the preliminary modeling helps to get early insight on how compound **5b** prevents the ASIC1a from sensing protons. To the best of our knowledge, there are no small molecules with reported pH-sensor binding.

Endogenous ASIC1a has primarily somatodendritic localization and is particularly enriched in brain synaptosomes and dendritic spines, suggesting that ASIC1a is presented in synapses.[67] Activation of ASIC1a should modulate synaptic responses and influence synaptic plasticity. It was shown that genetic disruption of ASIC impaired long-term synaptic plasticity in CA1 region of hippocampus[9] and lateral amygdala,[49] although another study showed that LTP can be generated in ASIC1a knockout mice.[10] These discrepancies may be due to the differences in strains and genetic deletion approaches. In our experiments compound **5b** did not affect baseline fEPSP, short-term plasticity, and NMDAR-independent LTP induced in MF-CA3 pathway but significantly impaired NMDAR-dependent LTP in CA1−CA3 pathway. Recent study indicates that presynaptic stimulation reduces extracellular pH and activates postsynaptic ASICs in the lateral amygdala synapses.[49] Activation of postsynaptic ASICs may lead to sodium influx into the postsynaptic terminal and depolarization of the postsynaptic membrane, which can be sensed in its turn by NMDARs in the neurons and thus potentiate their plasticity function.[9,68] The enhanced NMDAR response can facilitate the induction of long-term potentiation. The hypothesis that ASICs are required for the induction of NMDAR-dependent long-term potentiation was supported by two independent investigations using ASIC knockout mice in hippocampal formation and amygdala and by the fact that lowering magnesium can rescue LTP in the conditions of genetic ASIC ablation.[9,49] Our study further supports this assumption indicating that ASIC blockade selectively eliminates NMDAR-dependent LTP in CA3−CA1 synapses and does not affect NMDAR-independent LTP in MF-CA3 pathway.

CONCLUSION

Numerous pathological states and diseases including epilepsy, multiple sclerosis, ischemic disorders, traumatic brain injury, depression, spinal cord injury, inflammatory pain, and headache

DOI: 10.1021/jm5017329
J. Med. Chem. XXXX, XXX, XXX−XXX

are accompanied by tissue acidosis presumably activating ASIC1a. It has been shown that pharmacological blockage of ASIC1a as well as its genetic deletion or down regulation affects the above-mentioned pathological states, proving ASIC1a to be a promising molecular target against such disorders. Here we present a novel 2-oxo-2*H*-chromene-3-carboxamidine derivative compound **5b** which was designed by using molecular modeling approach to target pH sensor of ASIC1a channel. **5b** demonstrates its maximal potency in ASIC1a inhibition (nanomolar range) at physiologically attainable levels of pH. Our data indicate that compound **5b** acts as orthosteric noncompetitive antagonist of ASIC1a. Recent data on the role of ASIC1a in LTP are contradictory. The knockout data show that ASIC1a has a crucial role for NMDA-dependent LTP induction in hippocampus and learning ability.[9] However, other groups just by using different knockout approach came to a contradictory conclusion.[10] We found that novel orthosteric ASIC1a antagonist suppresses NMDA-dependent LTP and does not alter the NMDA-independent one. Our findings gave a new tool for determining the physiological and pathological role of ASIC1a channel. The suggested chemical scaffold can be used for the development of novel potent ASIC1a antagonists that can be used for the treatment of numerous brain diseases and pathologies.

EXPERIMENTAL SECTION

General Methods and Procedures. All chemicals were obtained from commercially available sources and used without further purification (Sigma-Aldrich, "Enamine LTD"). Solvents were purified and dried using standard methods. ^{1}H NMR spectra were recorded on a Varian Mercury-400 (400 MHz) instrument with TMS as internal standard. ^{13}C NMR spectra were obtained on a Bruker Avance DRX-500 spectrometer (125.75 MHz) with TMS as internal standard. The data are being reported as s = singlet, br s = broad singlet, d = doublet, t = triplet, q = quartet, and m = multiplet or unresolved; chemical shifts are in ppm and coupling constants in Hz. LC/MS spectra were recorded using chromatography/mass spectrometric system that consists of high-performance liquid chromatograph "Agilent 1100 series" equipped with diode-matrix and mass-selective detector "Agilent LC MSD SL". Elemental analysis was performed in the Microanalytical Laboratory of the Institute of Organic Chemistry, National Academy of Sciences of Ukraine. Compounds **6a**,**b**, **7a**, and **8a** are commercially available. Purity of all final compounds was 95% or higher.

All biological evaluation procedures were performed in accordance with the guidelines set by the National Institutes of Health for the Humane Treatment of Animals and approved by the Animal Care Committee of Bogomoletz Institute of Physiology.

Procedure a. Compounds 7c and 7d. A mixture of 3-aminophenol **6a**,**b** (0.01 mol), benzyl bromide (0.01 or 0.02 mol), and sodium bicarbonate (3.36g, 0.04 mol) in acetonitrile (150 mL) was stirred at 40 °C for 6 h. After cooling to room temperature, the reaction mixture was filtered and the filtrate evaporated under reduced pressure. Water (100 mL) and ethyl acetate (100 mL) were added to the residue. Organic layer was separated, washed with water, dried over Na_2SO_4, and the solvent was removed under reduced pressure. The product was used in the next step without further purification.

3-[Benzyl(methyl)amino]phenol (7c). Starting from 3-(methylamino)phenol **6b** and benzyl bromide (0.01 mol). Light brown oil. Yield 1.30 g (61%). ^{1}H NMR ($CDCl_3$,): δ = 2.98 (s, 3H, CH_3), 4.49 (s, 2H, CH_2), 6.22–6.30 (m, 2H), 6.34 (d, J = 8.0, 1H.), 7.05 (t, J = 8.0, 1H), 7.18–7.39 (m, 5H).

3-(Dibenzylamino)phenol (7d). Starting from 3-aminophenol **6a** and benzyl bromide (0.02 mol). Light yellow solid. Yield 2.25 g (78%). ^{1}H NMR (DMSO-d_6): δ = 4.60 (s, 4H, $2CH_2$), 6.01–6.13 (m, 3H), 6.82 (t, J = 8.0, 1H), 7.10–7.42 (m, 10H), 8.86 (s, 1H, OH).

Procedure b. Compounds 7b,e,f. A mixture of compound **6c** (2.45 g, 0.01 mol) and alkyl halide (0.01 mol) in acetonitrile (150 mL) was stirred at 81 °C for 3 h. After cooling to room temperature, the reaction mixture was evaporated under reduced pressure. Potassium carbonate aqueous solution (0.2 M, 100 mL) and dichloromethane (100 mL) were added to the residue. Organic layer was separated, washed with water, dried over Na_2SO_4, and the solvent was removed under reduced pressure. The product was used in the next step without further purification.

3-{[2-(Diethylamino)ethyl](ethyl)amino}phenol (7b). Using ethyl iodide as alkyl halide. Brown oil. Yield 0.94 g (40%). ^{1}H NMR ($CDCl_3$): δ = 1.08–1.19 (m, 9H, $3CH_3$), 2.64–2.75 (m, 6H, $3CH_2$), 3.32 (q, J = 7.2, 2H, CH_2), 3.40 (t, J = 7.0, 2H, CH_2), 6.20–6.29 (m, 3H), 7.03 (t, J = 8.0, 1H).

3-{Benzyl[2-(diethylamino)ethyl]amino}phenol (7e). Using benzyl chloride as alkyl halide. Brown oil. Yield 1.43 g (48%). ^{1}H NMR ($CDCl_3$): δ = 1.01 (t, J = 7.1, 6H, $2CH_3$), 2.57–2.64 (m, 6H, $3CH_2$), 3.50 (t, J = 7.1, 2H, CH_2), 4.46 (s, 2H, CH_2), 6.21–6.27 (m, 3H), 7.00–7.05 (m, 2H, H), 7.19 (d, J = 7.0, 2H), 7.26 (d, J = 7.0, 2H).

3-{(4-Chlorobenzyl)[2-(diethylamino)ethyl]amino}phenol (7f). Using 4-chlorobenzyl chloride as alkyl halide. Brown oil. Yield 1.57 g (47%). ^{1}H NMR ($CDCl_3$): δ = 1.04 (t, J = 7.0, 6H), 2.58 (q, J = 7.0, 4H), 2.69 (t, J = 7.2, 2H), 3.51 (t, J = 7.2, 2H), 4.48 (s, 2H), 6.13 (s, 1H), 6.22–6.27 (m, 2H), 7.02 (t, J = 8.5, 1H), 7.14 (d, J = 8.5, 2H), 7.28 (d, J = 8.5, 2H).

Procedure c. Compounds 8b–f. To the stirred ice-cooled dry dimethylformamide (2.2 mL) was slowly added freshly distilled phosphorus oxychloride (1.1 mL) via dropping funnel, and the mixture was stirred at 5 °C for 10 min. To this mixture a solution of **7b–f** (2 mmol) in dry dimethylformamide (2 mL) was slowly added under stirring at this temperature via dropping funnel. The mixture was allowed to warm to room temperature and then stirred additionally for 1 h. After this, the reaction mixture was heated to 80 °C for 2 h. After cooling, it was quenched with ice–water, mixed with charcoal (0.5 g), and filtered. To the clear solution saturated sodium bicarbonate solution was added, and the oil formed was extracted with ethyl acetate (20 mL). Organic layer was washed with brine, dried over sodium sulfate, and the solvent was evaporated. Compounds **8b–f** were obtained as dark brown oils and used for the next stage without additional purification.

4-{[2-(Diethylamino)ethyl](ethyl)amino}-2-hydroxybenzaldehyde (8b). Yield 0.40 g (75%). ^{1}H NMR ($CDCl_3$): δ = 1.11–1.16 (m, 9H, $3CH_3$), 2.60–2.66 (m, 6H, $3CH_2$), 3.39–3.47 (m, 4H, $2CH_2$), 6.11 (s, 1H), 6.36 (d, J = 8.0, 1H), 7.37 (d, J = 8.0, 1H), 9.56 (s, 1H, CHO), 11.70 (s, 1H, OH).

4-[Benzyl(methyl)amino]-2-hydroxybenzaldehyde (8c). Yield 0.38 g (79%). ^{1}H NMR ($CDCl_3$): δ = 3.12 (s, 3H, CH_3), 4.64 (s, 2H, CH_2), 6.18 (s, 1H), 6.35 (d, J = 8.0, 1H), 7.30–7.38 (m, 6H), 9.55 (s, 1H, CHO), 11.63 (s, 1H, OH).

4-(Dibenzylamino)-2-hydroxybenzaldehyde (8d). Yield 0.53 g (83%). ^{1}H NMR ($CDCl_3$): δ = 4.76 (s, 4H, $2CH_2$), 6.08 (s, 1H), 6.37 (d, J = 7.8, 1H), 7.30–7.45 (m, 11H), 9.61 (s, 1H, CHO), 11.11 (s, 1H, OH).

4-{Benzyl[2-(diethylamino)ethyl]amino}-2-hydroxybenzaldehyde (8e). Yield 0.51 (78%). ^{1}H NMR ($CDCl_3$): δ = 1.00 (t, J = 7.2, 6H, $2CH_3$), 2.52 (q, J = 7.2, 4H, $2CH_2$), 2.66 (t, J = 7.8, 2H, CH_2), 3.53 (t, J = 7.8, 2H, CH_2), 4.64 (s, 2H, CH_2), 6.11 (s, 1H), 6.30 (d, J = 8.4, 1H), 7.14 (d, J = 7.4, 2H), 7.24–7.31 (m, 4H), 9.45 (s, 1H, CHO), 11.54 (s, 1H, OH).

4-{(4-Chlorobenzyl)[2-(diethylamino)ethyl]amino}-2-hydroxybenzaldehyde (8f). Yield 0.58 g (80%). ^{1}H NMR ($CDCl_3$): δ = 1.01 (t, J = 6.9, 6H, $2CH_3$), 2.56 (q, J = 6.9, 4H, $2CH_2$), 2.66 (t, J = 7.1, 2H, CH_2), 3.54 (t, J = 7.1, 2H, CH_2), 4.63 (s, 2H, CH_2), 6.11 (s, 1H), 6.29 (d, J = 9.0, 1H), 7.10 (d, J = 7.4, 2H), 7.27–7.33 (m, 3H), 9.51 (s, 1H, CHO), 11.57 (s, 1H, OH).

Procedure d. Compounds 1–4, 5a,b. A mixture of **8a–f** (1 mmol), ammonium acetate (0.38 g, 5 mmol), and ethyl cyanoacetate (0.11 g, 1 mmol) in ethanol (5 mL) was refluxed for 10 min. After cooling, the mixture was diluted with diethyl ether (20 mL).

DOI: 10.1021/jm5017329
J. Med. Chem. XXXX, XXX, XXX–XXX

Precipitate formed was collected, washed with diethyl ether, dried in air, and triturated with saturated solution of sodium bicarbonate (5 mL) with stirring. The solid was filtered, washed with water, and dissolved in 2 N aqueous hydrochloric acid (5 mL). The mixture was evaporated to dryness under rotor vacuum. The light yellow solid residue of target compound was finally dried at 80 °C.

7-(Diethylamino)-2-oxo-2*H*-chromene-3-carboximidamide Hydrochloride (1). Using 4-(diethylamino)-2-hydroxybenzaldehyde **8a**. Yield 0.25 g (83%). Mp 255−257 °C. ^{1}H NMR (DMSO-d_6): δ = 1.17 (t, J = 7.2, 6H, $2CH_3$), 3.55 (q, J = 7.2, 4H, $2CH_2$), 6.63 (s, 1H), 6.90 (d, J = 8.0, 1H, $H_{arom.}$), 7.55 (d, J = 8.0, 1H), 8.93 (s, 1H), 9.15 (s, 4H, $2NH_2$). ^{13}C NMR (DMSO-d_6): δ = 12.23, 44.54, 95.96, 101.63, 107.04, 110.86, 131.98, 148.03, 153.72, 157.76, 159.20, 161.40. LC/MS (M + 1): 260. Elemental analysis calculated (%) for $C_{14}H_{18}ClN_3O_2$: C 56.85, H 6.13, Cl 11.99, N 14.21. Found: C 56.67, H 6.23, Cl 12.05, N 14.19.

7-{[2-(Diethylamino)ethyl](ethyl)amino}-2-oxo-2*H*-chromene-3-carboximidamide Dihydrochloride (2). Using 4-{[2-(diethylamino)ethyl](ethyl)amino}-2-hydroxybenzaldehyde **8b**. Yield 0.31 g (77%). Mp 188−190 °C. ^{1}H NMR (DMSO-d_6): δ = 1.17 (t, J = 7.0, 3H, CH_3), 1.27 (t, J = 7.0, 6H, $2CH_3$), 3.17−3.23 (m, 6H, $3CH_2$), 3.58 (q, J = 7.0, 2H, CH_2), 4.02 (t, J = 7.0, 2H, CH_2), 6.84 (s, 1H), 7.09 (d, J = 8.0, 1H, H), 7.57 (d, J = 8.0, 1H), 9.02 (s, 1H), 9.23 (s, 4H, $2NH_2$), 11.50 (s, 1H, NH^+). ^{13}C NMR (DMSO-d_6): δ = 8.33, 12.03, 44.38, 45.02, 46.01, 47.36, 96.88, 103.45, 107.66, 111.18,132.04, 148.42, 153.65, 157.43, 159.01, 161.47. LC/MS (M + 1): 331. Elemental analysis calculated (%) for $C_{18}H_{28}Cl_2N_4O_2$: C 53.60, H 7.00, Cl 17.58, N 13.89. Found: C 53.65, H 7.03, Cl 17.70, N 13.81.

7-[Benzyl(methyl)amino]-2-oxo-2*H*-chromene-3-carboximidamide Hydrochloride (3). Using 4-[benzyl(methyl)amino]-2-hydroxybenzaldehyde **8c**. Yield 0.28 g (80%). Mp 251−253 °C. ^{1}H NMR (DMSO-d_6): δ = 3.25 (s, 3H, CH_3), 4.82 (s, 2H, CH_2), 6.67 (s, 1H), 6.92 (d, J = 8.0, 1H), 7.23 (d, J = 7.0, 2H), 7.27 (t, J = 7.0, 1H), 7.36 (t, J = 7.0, 2H), 7.58 (d, J = 8.0, 1H), 8.89 (s, 1H), 9.16 (s, 4H, $2NH_2$). ^{13}C NMR (DMSO-d_6): δ = 39.50, 55.05, 96.88, 103.28, 107.47, 111.20, 126.48, 127.13, 128.65, 131.76, 137.05, 148.19, 155.14, 157.16, 158.98, 161.36. LC/MS (M + 1): 308. Elemental analysis calculated (%) for $C_{18}H_{18}ClN_3O_2$: C 62.88, H 5.28, Cl 10.31, N 12.22. Found: C 63.01, H 5.23, Cl 10.37, N 12.27.

7-(Dibenzylamino)-2-oxo-2*H*-chromene-3-carboximidamide Hydrochloride (4). Using 4-(dibenzylamino)phenol-2-hydroxybenzaldehyde **8d**. Yield 0.40 g (88%). Mp 288−290 °C. ^{1}H NMR (DMSO-d_6): δ = 4.92 (s, 4H, $2CH_2$), 6.61 (s, 1H), 6.87 (d, J = 8.0, 1H), 7.33−7.48 (m, 10H), 7.53 (d, J = 8.0, 1H), 8.99 (s, 1H), 9.17 (s, 4H, $2NH_2$). ^{13}C NMR (DMSO-d_6): δ = 55.10, 96.86, 103.21, 107.45, 111.24, 126.49, 127.11, 128.62, 131.77, 137.04, 148.13, 155.20, 157.18, 158.99, 161.36. LC/MS (M + 1): 384. Elemental analysis calculated (%) for $C_{24}H_{22}ClN_3O_2$: C 68.65, H 5.28, Cl 8.44, N 10.01. Found: C 68.60, H 5.21, Cl 8.51, N 9.96.

7-{Benzyl[2-(diethylamino)ethyl]amino}-2-oxo-2*H*-chromene-3-carboximidamide Dihydrochloride (5a). Using 4-{benzyl[2-(diethylamino)ethyl]amino}-2-hydroxybenzaldehyde **9e**. Yield 0.40 g (85%). Mp 192−194 °C. ^{1}H NMR (DMSO-d_6): δ = 1.24 (t, J = 7.0, 6H, $2CH_3$), 3.18 (q, J = 7.0, 4H, $2CH_2$), 3.29 (t, J = 7.2, 2H, CH_2), 4.16 (t, J = 7.2, 2H, CH_2), 4.88 (s, 2H, CH_2), 6.87 (s, 1H), 7.10 (d, J = 8.0, 1H), 7.24−7.30 (m, 3H), 7.35−7.41 (m, 2H), 7.60 (d, J = 9.2, 1H), 8.86 (s, 1H), 9.10 (s, 2H, NH_2), 9.23 (s, 2H, NH_2), 11.38 (s, 1H, NH^+). ^{13}C NMR (DMSO-d_6): δ = 8.34, 45.59, 45.99, 47.23, 53.45, 97.47, 104.69, 107.98, 111.33, 126.14, 126.97, 128.46, 131.70, 136.81, 148.18, 153.94, 157.07, 158.74, 161.39. LC/MS (M + 1): 393. Elemental analysis calculated (%) for $C_{23}H_{30}Cl_2N_4O_2$: C 59.36, H 6.50, Cl 15.23, N 12.04. Found: C 59.33, H 6.61, Cl 15.12, N 12.00.

7-{(4-Chlorobenzyl)[2-(diethylamino)ethyl]amino}-2-oxo-2*H*-chromene-3-carboximidamide Dihydrochloride (5b). Using 4-{(4-chlorobenzyl)[2-(diethylamino)ethyl]amino}-2-hydroxybenzaldehyde **9f**. Yield 0.42 g (84%). Mp 204−206 °C. ^{1}H NMR (DMSO-d_6): δ = 1.25 (t, J = 7.0, 6H, $2CH_3$).3.17 (q, J = 7.0, 4H, $2CH_2$), 3.29 (t, J = 7.4, 2H, CH_2), 4.15 (t, J = 7.4, 2H, CH_2), 4.87 (s, 2H, CH_2), 6.86 (s, 1H), 7.08 (d, J = 9.0, 1H), 7.27 (d, J = 8.5, 2H), 7.42 (d, J = 8.5, 2H), 7.59 (d, J = 9.0, 1H), 8.91 (s, 1H), 9.21 (s, 4H, $2NH_2$), 11.40 (s, 1H, NH^+). ^{13}C NMR (DMSO-d_6): δ = 8.31, 45.61, 46.03, 47.29, 52.83, 97.71, 104.99, 108.09, 111.42, 128.38, 128.65, 131.74, 131.96, 135.99, 148.22, 157.08, 158.72, 161.37. LC/MS (M + 1): 427. Elemental analysis calculated (%) for $C_{23}H_{29}Cl_3N_4O_2$: C 55.26, H 5.85, Cl 21.28, N 11.21. Found: C 55.17, H 5.82, Cl 21.30, N 11.25.

Homology Modeling and Structure Based Design. The structure of the human ASIC1a was modeled based on the crystal structure of chicken ASIC1a in the desensitized state solved at 1.9 Å resolution, 2QTS.[35] Sequences of human and chicken ASIC1a share high identity level (90.65%), which allows use of homology modeling with high confidence. Automated homology modeling routine of SWISS-MODEL server[69] was applied. Sequence of chicken ASIC1a was derived from UniProt database (UniProt code P78348). Transmembrane domains TM1 and TM2 of ASICs undergo major conformational transformations during channel function. In the crystal structure conformations of the three subunits are not equal, so we model every chain of human ASIC using corresponding chain from chicken ortholog (chains A, B, and C). Human has two amino acids insertion compared to chicken Asp298 and Leu299 which are located in the solvent exposed loop. Superposition of the Cα atoms of the ECDs (His74-Lys423, chicken numbering) omitting residues Asp297 and Ser298 from chicken and Asp296-Leu299 from human ASICs returned rmsd of 0.62 Å, which denotes reliability of the model. The full trimer was reconstructed by superposition of the model onto each monomer in the chicken model omitting transmembrane regions and the above-mentioned loop. In the generated model, positions of the side chain atoms were further energetically optimized using GROMACS, version 3.3, with OPLS 2001 force field in 5000 steps of conjugated gradient routine. The quality of the generated model was monitored using MolProbity server.[70]

Small molecule modeling and docking studies were performed with Schrodinger suite. Maestro was used for small molecule structure sketching and visualization of docking results.

For the pilot docking study we used Enamine diversity set, a library of 10 000 compounds selected basing on chemical structure diversity. Structures of small molecules were optimized with LigPrep module and their properties predicted with QuickProp. A-317567 was assumed to have trans conformation of its cyclopropyl group. Human ASIC1a structure was prepared with protein preparation wizard. Topologies of all atoms were reassigned and their positions were verified to prevent steric clashes. For docking studies, Glide module of Schrödinger was used. To generate a grid of the acidic pocket, amiloride molecule was manually inserted into the acidic pocket, and all residues within 25 Å from any amiloride atom were included in the grid generation. Conformations of small molecules were flexible, while protein atoms were fixed to their positions. For every generated pose postdocking minimization was performed and 10 complexes per structure were saved. To determine hydrophobic sites, SiteMap from Schrödinger suite was applied. The residues within 10 Å from bound A-317567 (as more extended ligand) were included in the calculation. Within isovalue cutoff of −0.58 only two regions in the pH sensor were detected (see Results).

HEK 293 Cells Culture. Human embryonic kidney 293 (HEK 293) cells (American Type Culture Collection, Manassas, VA, USA) were cultured in Dulbecco's modified Eagle medium (DMEM) supplemented with 10% fetal bovine serum and 10 U/mL penicillin and 10 mg/mL streptomycin (all from Invitrogen, USA). Dissociated cells were either replated for a new passage or used for patch clamp experiments. Cells were cultured at 37 °C under an atmosphere of 5% CO_2 and 95% air with approximately 95% humidity.

Hippocampal Slices Preparation. Acute temporal lobe slices including neocortical areas (Te2 and Te3), entorhinal cortex, subiculum, and hippocampus were prepared from Wistar rats aged postnatal days 19−21 (P19−21) as previously described with some modifications.[71] On the day of experiment, a rat was deeply anesthetized using sevoflurane and decapitated. Cerebellum, frontal lobe region (coronal section), and ventral-lateral areas (sections at the angle 20−30° off the horizontal axis) were removed from the brain.

DOI: 10.1021/jm5017329
J. Med. Chem. XXXX, XXX, XXX−XXX

The remaining part of the brain was mounted on the stage of a Vibroslice NVSL (World Precision Instruments Inc., Sarasota, FL, USA) and cut (400 μm) through the hemispheres at an angle of 30−35° of their horizontal planes. All manipulations were performed in freshly prepared ice-cold oxygenated (95% O_2−5% CO_2) artificial cerebrospinal fluid (ACSF) of the following composition (mM): NaCl 119, KCl 2.5, $CaCl_2$ 2.0, $MgSO_4$ 1.3, $NaHCO_3$ 26, NaH_2PO_4 1.0, and glucose 11 (pH 7.35). For the experiments we took 3−4 slices from the septal (dorsal) part of the hippocampus.[72] Slices were maintained in an oxygenated ACSF at a room temperature for at least 1.5 h before use.

Electrophysiological Recordings. Whole cell patch clamp recordings were made with EPC-8/LIH 1600 amplifier/acquisition system; data were collected using PatchMaster software (all from HEKA, Lambrecht/Pfalz, Germany). Current was recorded at holding potential of −100 mV, unless otherwise indicated. Current traces were samples at 10 kHz and filtered online at 3 kHz. Patch electrodes (2−3 MΩ) were filled with a solution containing the following (in mM): 120 KF, 20 Tris-Cl, (adjusted to pH 7.3 with KOH). Extracellular solution contained the following (in mM): 130 NaCl, 5 KCl, 2 $MgCl_2$, 2 $CaCl_2$, 20 HEPES/NaOH, pH 7.4. A fully automated "jumping table" setup (PharmaRobot, Kiev, Ukraine) was used for applications of external solutions (see ref 73).

Brain slices were transferred to the incubation chamber and superfused with oxygenated ACSF at a rate of 2 mL/min (22−24 °C). Extracellular recordings of fEPSP were obtained using extracellular glass microelectrodes (3−4 MΩ) filled with ACSF and patch-clamp amplifier (PC 501A, Warner Instruments Corp., Hamden, CT, or RK-400, BioLogic, France). To induce NMDAR-dependent or NMDAR-independent long-term potentiation (LTP), evoked postsynaptic responses were elicited by stimulation of Schaffer collateral-commissural pathway or mossy-fibers (MF) and recordings have been made within the CA1 stratum radiatum (SR) or CA3 stratum lucidum (SL) of hippocampus, respectively. Stimulating and recording electrodes were placed on the slice surface approximately 400 μm apart from each other. Stimulation was performed using a concentric bipolar stimulating electrode (FHC Inc., Bowdoin, ME) connected to a flexible stimulus isolator (ISO-Flex, A.M.P. Instruments, Jerusalem, Israel). Stimulation intensity varied between 150 and 400 μA in all slices. For baseline recording of fEPSP, stimulation was applied every 20 s at the intensity sufficient to elicit 30% of maximal response. The stimulation protocol to induce synaptic plasticity was applied after 10−15 min of stable baseline recording. To induce LTP, high-frequency tetanic stimulation (HFS) was delivered at baseline stimulation intensity (100 pulses at frequency of 100 Hz for NMDAR-dependent LTP and 4 bursts of 100 pulses at 100 Hz with a 2 min interval for NMDAR-independent LTP). MF-CA3 LTP recordings were performed in the presence of 1 μM MK-801 ((5*S*,10*R*)-(+)-5-methyl-10,11-dihydro-5*H*-dibenzo[*a*,*d*]cyclohepten-5,10-imine maleate). Recordings were digitized at 10 kHz using an analogue-to-digital converter (NI PCI-6221, National Instruments, Austin, TX) and stored on a computer using the WinWCP program (Strathclyde Electrophysiology Software, University of Strathclyde, Glasgow, U.K.) or custom software written in Labview 8.0 (National Instruments, Austin, TX).

Data Analysis. Off-line analysis was performed using Clampfit (Axon Instruments, USA), Prism 5 (GraphPad, La Jolla, CA), and Origin 7.5 (OriginLab, Northampton, MA) software. The 50% inhibitory concentrations (IC_{50}) was determined by analyzing the log of the concentration−response curves by nonlinear regression analysis. Two-way repeated measures ANOVA and unpaired Student's *t* test were used to analyze changes in postsynaptic response. Results were expressed as the mean ± SEM; *n* is the number of recordings.

■ ASSOCIATED CONTENT

Ⓢ Supporting Information

Additional figures illustrating 3D crystal structure of ASIC1a channel, superpositions and alignment of different molecules in pH sensor, and electrophysiological evaluation of compound **5b** on hippocampal neurons and slices. The Supporting Information is available free of charge on the ACS Publications website at DOI: 10.1021/jm5017329.

■ AUTHOR INFORMATION

Corresponding Author

*E-mail: krishtal@biph.kiev.ua. Phone: +380 44 2532466. Fax: +380 44 2562590.

Present Address

[#]D.K.: Department of Biochemistry, University of Texas Health Science Center, 7703 Floyd Curl Drive, San Antonio, TX 78229-3900, U.S.

Author Contributions

[⊥]O.M., D.K., and V.S. contributed equally.

The authors have made the following declarations about their contributions. Conceived and designed the experiments: O.M., E.I., O.K., D.I., M.V., V.S. Performed the experiments: A.B., V.S., E.I., A.S. Performed the modeling studies: D.K. Analyzed the data: O.M., E.I. Wrote the paper: O.M., O.K., V.S., D.K., D.I. Conceived and conducted the study: O.K., O.M., D.K., V.S. All authors have given approval to the final version of the manuscript.

Notes

The authors declare no competing financial interest.

■ ACKNOWLEDGMENTS

This work was supported in part by the NIH (Grant lR03TW008228-01A1) and Ukrainian government (State Target Scientific and Technical Program "Nanotechnology and Nanomaterials" for 2010−2014)

■ ABBREVIATIONS USED

ASIC, acid sensing ion channel; NMDAR, *N*-methyl-D-aspartate receptor; LTP, long-term potentiation; NSAID, nonsteroidal anti-inflammatory drug; ENaC, epithelial sodium channel; DAPI, 4′,6-diamidino-2-phenylindole; fEPSP, field excitatory postsynaptic potential; eEPSC, evoked excitatory postsynaptic currents; eIPSC, evoked inhibitory postsynaptic currents; STP, short-term potentiation; ACSF, artificial cerebrospinal fluid; DMEM, Dulbecco's modified Eagle medium; HEK 293, human embryonic kidney 293; HEPES, 4-(2-hydroxyethyl)-1-piperazineethanesulfonic acid

■ REFERENCES

(1) Grunder, S.; Chen, X. Structure, function, and pharmacology of acid-sensing ion channels (ASICs): focus on ASIC1a. *Int. J. Physiol., Pathophysiol. Pharmacol.* **2010**, *2*, 73−94.

(2) Waldmann, R.; Champigny, G.; Bassilana, F.; Heurteaux, C.; Lazdunski, M. A proton-gated cation channel involved in acid-sensing. *Nature* **1997**, *386*, 173−177.

(3) Wemmie, J. A.; Price, M. P.; Welsh, M. J. Acid-sensing ion channels: advances, questions and therapeutic opportunities. *Trends Neurosci.* **2006**, *29*, 578−586.

(4) Feldman, D. H.; Horiuchi, M.; Keachie, K.; McCauley, E.; Bannerman, P.; Itoh, A.; Itoh, T.; Pleasure, D. Characterization of acid-sensing ion channel expression in oligodendrocyte-lineage cells. *Glia* **2008**, *56*, 1238−1249.

(5) Yermolaieva, O.; Leonard, A. S.; Schnizler, M. K.; Abboud, F. M.; Welsh, M. J. Extracellular acidosis increases neuronal cell calcium by activating acid-sensing ion channel 1a. *Proc. Natl. Acad. Sci. U.S.A.* **2004**, *101*, 6752−6757.

(6) Babini, E.; Paukert, M.; Geisler, H. S.; Grunder, S. Alternative splicing and interaction with di- and polyvalent cations control the

DOI: 10.1021/jm5017329
J. Med. Chem. XXXX, XXX, XXX−XXX

dynamic range of acid-sensing ion channel 1 (ASIC1). *J. Biol. Chem.* **2002**, *277*, 41597−41603.
(7) Ziemann, A. E.; Allen, J. E.; Dahdaleh, N. S.; Drebot, II; Coryell, M. W.; Wunsch, A. M.; Lynch, C. M.; Faraci, F. M.; Howard, M. A., 3rd; Welsh, M. J.; Wemmie, J. A. The amygdala is a chemosensor that detects carbon dioxide and acidosis to elicit fear behavior. *Cell* **2009**, *139*, 1012−1021.
(8) Krishtal, O. The ASICs: signaling molecules? Modulators? *Trends Neurosci.* **2003**, *26*, 477−483.
(9) Wemmie, J. A.; Chen, J.; Askwith, C. C.; Hruska-Hageman, A. M.; Price, M. P.; Nolan, B. C.; Yoder, P. G.; Lamani, E.; Hoshi, T.; Freeman, J. H., Jr.; Welsh, M. J. The acid-activated ion channel ASIC contributes to synaptic plasticity, learning, and memory. *Neuron* **2002**, *34*, 463−477.
(10) Wu, P. Y.; Huang, Y. Y.; Chen, C. C.; Hsu, T. T.; Lin, Y. C.; Weng, J. Y.; Chien, T. C.; Cheng, I. H.; Lien, C. C. Acid-sensing ion channel-1a is not required for normal hippocampal LTP and spatial memory. *J. Neurosci.* **2013**, *33*, 1828−1832.
(11) Yin, T.; Lindley, T. E.; Albert, G. W.; Ahmed, R.; Schmeiser, P. B.; Grady, M. S.; Howard, M. A.; Welsh, M. J. Loss of acid sensing ion channel-1a and bicarbonate administration attenuate the severity of traumatic brain injury. *PLoS One* **2013**, *8*, e72379.
(12) Chu, X. P.; Xiong, Z. G. Acid-sensing ion channels in pathological conditions. *Adv. Exp. Med. Biol.* **2013**, *961*, 419−431.
(13) Dube, G. R.; Lehto, S. G.; Breese, N. M.; Baker, S. J.; Wang, X.; Matulenko, M. A.; Honore, P.; Stewart, A. O.; Moreland, R. B.; Brioni, J. D. Electrophysiological and in vivo characterization of A-317567, a novel blocker of acid sensing ion channels. *Pain* **2005**, *117*, 88−96.
(14) Kuduk, S. D.; Chang, R. K.; Di Marco, C. N.; Dipardo, R. M.; Cook, S. P.; Cato, M. J.; Jovanovska, A.; Urban, M. O.; Leitl, M.; Spencer, R. H.; Kane, S. A.; Hartman, G. D.; Bilodeau, M. T. Identification of non-amidine inhibitors of acid-sensing ion channel-3 (ASIC3). *Bioorg. Med. Chem. Lett.* **2011**, *21*, 4255−4258.
(15) Kuduk, S. D.; Chang, R. K.; Wai, J. M.; Di Marco, C. N.; Cofre, V.; DiPardo, R. M.; Cook, S. P.; Cato, M. J.; Jovanovska, A.; Urban, M. O.; Leitl, M.; Spencer, R. H.; Kane, S. A.; Hartman, G. D.; Bilodeau, M. T. Amidine derived inhibitors of acid-sensing ion channel-3 (ASIC3). *Bioorg. Med. Chem. Lett.* **2009**, *19*, 4059−4063.
(16) Kuduk, S. D.; Di Marco, C. N.; Chang, R. K.; Dipardo, R. M.; Cook, S. P.; Cato, M. J.; Jovanovska, A.; Urban, M. O.; Leitl, M.; Spencer, R. H.; Kane, S. A.; Bilodeau, M. T.; Hartman, G. D.; Bock, M. G. Amiloride derived inhibitors of acid-sensing ion channel-3 (ASIC3). *Bioorg. Med. Chem. Lett.* **2009**, *19*, 2514−2518.
(17) Chen, X.; Orser, B. A.; MacDonald, J. F. Design and screening of ASIC inhibitors based on aromatic diamidines for combating neurological disorders. *Eur. J. Pharmacol.* **2010**, *648*, 15−23.
(18) Qadri, Y. J.; Rooj, A. K.; Fuller, C. M. ENaCs and ASICs as therapeutic targets. *Am. J. Physiol.: Cell Physiol.* **2012**, *302*, C943−C965.
(19) Deval, E.; Gasull, X.; Noel, J.; Salinas, M.; Baron, A.; Diochot, S.; Lingueglia, E. Acid-sensing ion channels (ASICs): pharmacology and implication in pain. *Pharmacol. Ther.* **2010**, *128*, 549−558.
(20) Korkushko, A. O.; Kryshtal, O. A. [Blocking of proton-activated sodium permeability of the membranes of trigeminal ganglion neurons in the rat by organic cations]. *Neirofiziologiia* **1984**, *16*, 557−561.
(21) Alvarez de la Rosa, D.; Canessa, C. M.; Fyfe, G. K.; Zhang, P. Structure and regulation of amiloride-sensitive sodium channels. *Annu. Rev. Physiol.* **2000**, *62*, 573−594.
(22) Schild, L.; Schneeberger, E.; Gautschi, I.; Firsov, D. Identification of amino acid residues in the alpha, beta, and gamma subunits of the epithelial sodium channel (ENaC) involved in amiloride block and ion permeation. *J. Gen. Physiol.* **1997**, *109*, 15−26.
(23) Kellenberger, S.; Gautschi, I.; Schild, L. Mutations in the epithelial Na^+ channel ENaC outer pore disrupt amiloride block by increasing its dissociation rate. *Mol. Pharmacol.* **2003**, *64*, 848−856.
(24) Ciampolillo, F.; McCoy, D. E.; Green, R. B.; Karlson, K. H.; Dagenais, A.; Molday, R. S.; Stanton, B. A. Cell-specific expression of amiloride-sensitive, Na(+)-conducting ion channels in the kidney. *Am. J. Physiol.* **1996**, *271*, C1303−C1315.
(25) Pouyssegur, J.; Chambard, J. C.; Franchi, A.; Paris, S.; Van Obberghen-Schilling, E. Growth factor activation of an amiloride-sensitive Na^+/H^+ exchange system in quiescent fibroblasts: coupling to ribosomal protein S6 phosphorylation. *Proc. Natl. Acad. Sci. U.S.A.* **1982**, *79*, 3935−3939.
(26) Tang, C. M.; Presser, F.; Morad, M. Amiloride selectively blocks the low threshold (T) calcium channel. *Science* **1988**, *240*, 213−215.
(27) Vassalli, J. D.; Belin, D. Amiloride selectively inhibits the urokinase-type plasminogen activator. *FEBS Lett.* **1987**, *214*, 187−191.
(28) Kuduk, S. D.; Di Marco, C. N.; Bodmer-Narkevitch, V.; Cook, S. P.; Cato, M. J.; Jovanovska, A.; Urban, M. O.; Leitl, M.; Sain, N.; Liang, A.; Spencer, R. H.; Kane, S. A.; Hartman, G. D.; Bilodeau, M. T. Synthesis, structure-activity relationship, and pharmacological profile of analogs of the ASIC-3 inhibitor A-317567. *ACS Chem. Neurosci.* **2010**, *1*, 19−24.
(29) Ugawa, S.; Ishida, Y.; Ueda, T.; Inoue, K.; Nagao, M.; Shimada, S. Nafamostat mesilate reversibly blocks acid-sensing ion channel currents. *Biochem. Biophys. Res. Commun.* **2007**, *363*, 203−208.
(30) Chen, X.; Qiu, L.; Li, M.; Durrnagel, S.; Orser, B. A.; Xiong, Z. G.; MacDonald, J. F. Diarylamidines: high potency inhibitors of acid-sensing ion channels. *Neuropharmacology* **2010**, *58*, 1045−1053.
(31) Wolkenberg, S. E.; Zhao, Z.; Mulhearn, J. J.; Harrison, S. T.; Sanders, J. M.; Cato, M. J.; Jovanovska, A.; Panigel, J.; Cook, S. P.; Henze, D. A.; Kane, S. A.; Hartman, G. D.; Barrow, J. C. High concentration electrophysiology-based fragment screen: discovery of novel acid-sensing ion channel 3 (ASIC3) inhibitors. *Bioorg. Med. Chem. Lett.* **2011**, *21*, 2646−2649.
(32) Voilley, N.; de Weille, J.; Mamet, J.; Lazdunski, M. Nonsteroid anti-inflammatory drugs inhibit both the activity and the inflammation-induced expression of acid-sensing ion channels in nociceptors. *J. Neurosci.* **2001**, *21*, 8026−8033.
(33) Leng, T.; Lin, J.; Cottrell, J. E.; Xiong, Z. G. Subunit and frequency-dependent inhibition of acid sensing ion channels by local anesthetic tetracaine. *Mol. Pain* **2013**, *9*, 27.
(34) Lin, J.; Chu, X.; Maysami, S.; Li, M.; Si, H.; Cottrell, J. E.; Simon, R. P.; Xiong, Z. Inhibition of acid sensing ion channel currents by lidocaine in cultured mouse cortical neurons. *Anesth. Analg.* **2011**, *112*, 977−981.
(35) Jasti, J.; Furukawa, H.; Gonzales, E. B.; Gouaux, E. Structure of acid-sensing ion channel 1 at 1.9 Å resolution and low pH. *Nature* **2007**, *449*, 316−323.
(36) Gonzales, E. B.; Kawate, T.; Gouaux, E. Pore architecture and ion sites in acid-sensing ion channels and P2X receptors. *Nature* **2009**, *460*, 599−604.
(37) Baconguis, I.; Gouaux, E. Structural plasticity and dynamic selectivity of acid-sensing ion channel-spider toxin complexes. *Nature* **2012**, *489*, 400−405.
(38) Baconguis, I.; Bohlen, C. J.; Goehring, A.; Julius, D.; Gouaux, E. X-ray structure of acid-sensing ion channel 1-snake toxin complex reveals open state of a Na(+)-selective channel. *Cell* **2014**, *156*, 717−729.
(39) Dawson, R. J.; Benz, J.; Stohler, P.; Tetaz, T.; Joseph, C.; Huber, S.; Schmid, G.; Hugin, D.; Pflimlin, P.; Trube, G.; Rudolph, M. G.; Hennig, M.; Ruf, A. Structure of the acid-sensing ion channel 1 in complex with the gating modifier psalmotoxin 1. *Nat. Commun.* **2012**, *3*, 936.
(40) Escoubas, P.; De Weille, J. R.; Lecoq, A.; Diochot, S.; Waldmann, R.; Champigny, G.; Moinier, D.; Menez, A.; Lazdunski, M. Isolation of a tarantula toxin specific for a class of proton-gated Na^+ channels. *J. Biol. Chem.* **2000**, *275*, 25116−25121.
(41) Bonifacio, G.; Lelli, C. I.; Kellenberger, S. Protonation controls ASIC1a activity via coordinated movements in multiple domains. *J. Gen. Physiol.* **2014**, *143*, 105−118.
(42) Elslager, E. F.; Worth, D. F. Synthetic schistosomicides. XVI. 5-(Mono- and dialkylamino)-2-nitrosophenols, 2-amino-5-(dialkylamino)phenols, and related compounds. *J. Med. Chem.* **1970**, *13*, 370−376.
(43) Sakurai, A.; Midorikawa, H.; Hashimoto, Y. The cyclization of ethyl cyanoacetate and salicylaldehyde or 3-methoxysalicylaldehyde

DOI: 10.1021/jm5017329
J. Med. Chem. XXXX, XXX, XXX−XXX

with ketones by means of ammonium acetate. *Bull. Chem. Soc. Jpn.* **1970**, *43*, 2925−2933.
(44) Lunko, O.; Isaev, D.; Maximyuk, O.; Ivanchick, G.; Sydorenko, V.; Krishtal, O.; Isaeva, E. Persistent sodium current properties in hippocampal CA1 pyramidal neurons of young and adult rats. *Neurosci. Lett.* **2014**, *559*, 30−33.
(45) Gunthorpe, M. J.; Smith, G. D.; Davis, J. B.; Randall, A. D. Characterisation of a human acid-sensing ion channel (hASIC1a) endogenously expressed in HEK293 cells. *Pfluegers Arch.* **2001**, *442*, 668−674.
(46) Sukach, V. A.; Buta, A. Z.; Maksymiuk, O. P.; Koval's'kyi, D. B.; Vovk, M. V.; Kryshtal, O. O. [(3-carboxamidino-2-oxo-2H-chromen-7-yl)-4-guanidinobenzoates are novel blockers of pH-sensitive ion channels]. *Fiziol. Zh.* **2011**, *57*, 31−37.
(47) *SiteMap*, version 2.3; Schrodinger, LLC: New York, NY, 2009.
(48) Kenakin, T. P. Drug Antagonism: Orthosteric Drug Effects. In *Pharmacology in Drug Discovery: Understanding Drug Response*; Academic Press: Amsterdam, 2011; pp 67−97.
(49) Du, J.; Reznikov, L. R.; Price, M. P.; Zha, X. M.; Lu, Y.; Moninger, T. O.; Wemmie, J. A.; Welsh, M. J. Protons are a neurotransmitter that regulates synaptic plasticity in the lateral amygdala. *Proc. Natl. Acad. Sci. U.S.A.* **2014**, *111*, 8961−8966.
(50) Urban, N. N.; Barrionuevo, G. Induction of hebbian and non-hebbian mossy fiber long-term potentiation by distinct patterns of high-frequency stimulation. *J. Neurosci.* **1996**, *16*, 4293−4299.
(51) Krishtal, O. A.; Pidoplichko, V. I. A "receptor" for protons in small neurons of trigeminal ganglia: possible role in nociception. *Neurosci. Lett.* **1981**, *24*, 243−246.
(52) Krishtal, O. A.; Pidoplichko, V. I. Receptor for protons in the membrane of sensory neurons. *Brain Res.* **1981**, *214*, 150−154.
(53) Krishtal, O. A.; Pidoplichko, V. I. A receptor for protons in the membrane of sensory neurons may participate in nociception. *Neuroscience* **1981**, *6*, 2599−2601.
(54) Akopian, A. N.; Chen, C. C.; Ding, Y.; Cesare, P.; Wood, J. N. A new member of the acid-sensing ion channel family. *NeuroReport* **2000**, *11*, 2217−2222.
(55) Grunder, S.; Geissler, H. S.; Bassler, E. L.; Ruppersberg, J. P. A new member of acid-sensing ion channels from pituitary gland. *NeuroReport* **2000**, *11*, 1607−1611.
(56) Lingueglia, E.; de Weille, J. R.; Bassilana, F.; Heurteaux, C.; Sakai, H.; Waldmann, R.; Lazdunski, M. A modulatory subunit of acid sensing ion channels in brain and dorsal root ganglion cells. *J. Biol. Chem.* **1997**, *272*, 29778−29783.
(57) Waldmann, R.; Bassilana, F.; de Weille, J.; Champigny, G.; Heurteaux, C.; Lazdunski, M. Molecular cloning of a non-inactivating proton-gated Na^+ channel specific for sensory neurons. *J. Biol. Chem.* **1997**, *272*, 20975−20978.
(58) Wemmie, J. A.; Taugher, R. J.; Kreple, C. J. Acid-sensing ion channels in pain and disease. *Nat. Rev. Neurosci.* **2013**, *14*, 461−471.
(59) Benarroch, E. E. Acid-sensing cation channels: structure, function, and pathophysiologic implications. *Neurology* **2014**, *82*, 628−635.
(60) Kweon, H. J.; Suh, B. C. Acid-sensing ion channels (ASICs): therapeutic targets for neurological diseases and their regulation. *BMB Rep.* **2013**, *46*, 295−304.
(61) Sherwood, T. W.; Frey, E. N.; Askwith, C. C. Structure and activity of the acid-sensing ion channels. *Am. J. Physiol.: Cell Physiol.* **2012**, *303*, C699−C710.
(62) Klumpp, K.; Graves, B. J. Optimization of small molecule drugs binding to highly polar target sites: lessons from the discovery and development of neuraminidase inhibitors. *Curr. Top. Med. Chem.* **2006**, *6*, 423−34.
(63) Liechti, L. A.; Berneche, S.; Bargeton, B.; Iwaszkiewicz, J.; Roy, S.; Michielin, O.; Kellenberger, S. A combined computational and functional approach identifies new residues involved in pH-dependent gating of ASIC1a. *J. Biol. Chem.* **2010**, *285*, 16315−16329.
(64) Chen, X.; Kalbacher, H.; Grunder, S. The tarantula toxin psalmotoxin 1 inhibits acid-sensing ion channel (ASIC) 1a by increasing its apparent H^+ affinity. *J. Gen. Physiol.* **2005**, *126*, 71−79.
(65) Chen, X.; Kalbacher, H.; Grunder, S. Interaction of acid-sensing ion channel (ASIC) 1 with the tarantula toxin psalmotoxin 1 is state dependent. *J. Gen. Physiol.* **2006**, *127*, 267−276.
(66) Jiang, Q.; Li, M. H.; Papasian, C. J.; Branigan, D.; Xiong, Z. G.; Wang, J. Q.; Chu, X. P. Characterization of acid-sensing ion channels in medium spiny neurons of mouse striatum. *Neuroscience* **2009**, *162*, 55−66.
(67) Zha, X. M. Acid-sensing ion channels: trafficking and synaptic function. *Mol. Brain* **2013**, *6*, 1.
(68) Yu, X. M.; Salter, M. W. Gain control of NMDA-receptor currents by intracellular sodium. *Nature* **1998**, *396*, 469−474.
(69) Arnold, K.; Bordoli, L.; Kopp, J.; Schwede, T. The SWISS-MODEL workspace: a web-based environment for protein structure homology modelling. *Bioinformatics* **2006**, *22*, 195−201.
(70) Davis, I. W.; Leaver-Fay, A.; Chen, V. B.; Block, J. N.; Kapral, G. J.; Wang, X.; Murray, L. W.; Arendall, W. B., 3rd; Snoeyink, J.; Richardson, J. S.; Richardson, D. C. MolProbity: all-atom contacts and structure validation for proteins and nucleic acids. *Nucleic Acids Res.* **2007**, *35*, W375−W383.
(71) Isaev, D.; Ivanchick, G.; Khmyz, V.; Isaeva, E.; Savrasova, A.; Krishtal, O.; Holmes, G. L.; Maximyuk, O. Surface charge impact in low-magnesium model of seizure in rat hippocampus. *J. Neurophysiol.* **2012**, *107*, 417−423.
(72) Papatheodoropoulos, C.; Kostopoulos, G. Decreased ability of rat temporal hippocampal CA1 region to produce long-term potentiation. *Neurosci. Lett.* **2000**, *279*, 177−180.
(73) Khmyz, V.; Maximyuk, O.; Teslenko, V.; Verkhratsky, A.; Krishtal, O. P2X3 receptor gating near normal body temperature. *Pfluegers Arch.* **2008**, *456*, 339−347.

DOI: 10.1021/jm5017329
J. Med. Chem. XXXX, XXX, XXX−XXX